Journal of Physics and Chemistry of Solids

Volume 74, Issue 1, Pages 1-174 (January 2013)

Simple metal binary phases based on the body centered cubic structure: Electronic origin of distortions and superlattices

Original Research Article
Pages 18-24
Valentina F. Degtyareva, Nataliya S. Afonikova

Highlights

► We consider complex binary phases of simple metals related to the body centered structures. ► Crystal structure of these phases is shown to be stabilized due to electron band structure energy. ► We analyze Fermi sphere–Brillouin zone configurations within the Hume-Rothery mechanism. ► This approach may be useful in understanding complex phases found in compressed alkali metals.

First-principles study on electronic structure and optical properties of $Ca_4Bi_6O_{13}$ crystal

Original Research Article
Pages 25-29
Hiroyuki Nakamura, Yuki Obukuro, Kenji Obata, Shigenori Matsushima, Masao Arai, Kenkichiro Kobayashi

Highlights

► The electronic structure of $Ca_4Bi_6O_{13}$ is firstly clarified on the basis of DFT–GGA. ► The optical properties of $Ca_4Bi_6O_{13}$ are theoretically described in details. ► The theoretical results are discussed from the view point of photocatalyst.

A detailed study of scaling behavior in electrochemical etching of tungsten wires: Effects of non-uniform etching

Original Research Article
Pages 30-34
P. McDonnell, T. Graveson, C. Rackson, W.J. Kim

Highlights

► We have performed electrochemical etching of tungsten wires. ► A slightly reduced scaling exponent is observed from electrical resistance measurements. ► Surface inhomogeneity is shown to be responsible for the reduced scaling exponent. ► Despite inhomogeneity, the obtained exponent is consistent with a previous study.

Oscillations of transport properties in $PbTe–Bi_2Te_3$ solid solutions

Original Research Article
Pages 35-39
E.I. Rogacheva, O.S. Vodorez, O.N. Nashchekina

Highlights

► Concentration dependences of properties in PbTe-based solid solution have oscillatory character. ► The observed effects are attributed to percolation phenomena and self-organization processes. ► It is suggested that the observed phenomena are typical for a wide range of solid solutions.

Growth of germanium nanowires from bis(acetylacetonato) dichloro germanium

Original Research Article
Pages 40-44
A. Hammami, C.F. Garnero, G. Brewer, D.A. McKeown, A. Buechele, I.L. Pegg, J. Philip

Highlights

► We have synthesized a novel precursor for the growth of high quality germanium nanowires. ► Bis(acetylacetonato) dichloro germanium is used as the precursor for the growth of Ge nanowires. ► This precursor is solid and stable at room temperature. ► It can be used to grow germanium at fairly low temperatures (~400 °C) and on a variety of substrates.

A simplified approach to the band gap correction of defect formation energies: Al, Ga, and In-doped ZnO

Original Research Article
Pages 45-50
R. Saniz, Y. Xu, M. Matsubara, M.N. Amini, H. Dixit, D. Lamoen, B. Partoens

Highlights

► We introduce a new scheme to calculate the formation energies of defect systems. ► Our method compares very well with proven, but computationally heavier, methods. ► We investigate systematically ZnO doped with group III elements (Al, Ga, In). ► All three dopants are shallow donors, with a preferred charge state is +1. ► Substitutional doping is energetically favorable, compared to interstitial doping.

Optoelectrical and magnetic characteristics of Mn doped $Zn_{1-x}Sn_xO$ nanorods

Original Research Article
Pages 51-56
Tsung-Yin Hsu, Shang-Hung Lai, Hui-Huang Hsieh, Ming-Der Lan, Chih-Chuan Su, Mon-Shu Ho

Highlights

► $Zn_{1-x}Sn_xO$ nanorods were fabricated on Si with VLS mechanism in MLD process. ► The band gap of single doped-ZnO nanorods was determined by C-AFM to be 3–3.45 eV. ► Mn doped $Zn_{1-x}Sn_xO$ nanorods have superior UV emissions at 363 nm peak. ► The character of Mn doped $Zn_{1-x}Sn_xO$ nanorods presents the applicability in DMS.

Sources of carrier compensation in arsenic-doped HgCdTe

Original Research Article
Pages 57-64
H. Duan, Y.Z. Dong, J. Luo, Y. Huang, X.S. Chen, W. Lu

Highlights

► We calculated the electronic properties and stability of Hg-vacancies defects in As-doped HgCdTe. ► The Hg-vacancies defects that relate to carrier compensation in As-doped HgCdTe are confirmed. ► The role of Hg-vacancies defects in arsenic activation is discussed. ► More convinced model for arsenic doping is provided.

Influence of immersion cycles on the stoichiometry of CdS films deposited by SILAR technique

Original Research Article
Pages 65-69
V. Senthamilselvi, K. Ravichandran, K. Saravanakumar

Highlights

► Good quality CdS films with near stoichiometry are realized. ► It is achieved by introducing fresh solution in the final cycles of the dipping process. ► This study is the first of its kind in the SILAR process. ► Stoichiometry is suitably correlated with structural, optical and surface properties.

Effect of KOH on glycine phosphite single crystal grown by the SR

method

Original Research Article
Pages 70-74
S. Supriya, S. Kalainathan, G. Bhagavannarayana

Highlights

► KOH doped GPI single crystal has been grown by the SR method for the first time and confirmed by XRD. ► Dielectric studies of KOH-GPI shows high curie temperature value comparing with pure GPI. ► The crystal structure of SR method grown pure and KOH doped GPI crystal was analyzed from HRXRD data. ► The optical property of both samples was studied by the UV–visible spectrum.

Grain size effects on the compressibility and yield strength of copper

Original Research Article
Pages 75-79
Yuejian Wang, Jianzhong Zhang, Qiang Wei, Yusheng Zhao

Highlights

► Copper with different grain sizes was investigated under extreme conditions. ► The mechanical properties were obtained through the evaluation of X-ray profiles. ► The strength of copper was substantially increased by the reduction of grain sizes. ► This research is important for better understanding of the natures of fcc metals.

p-type ZnO films prepared by alternate deposition of ZnO and Mg_3N_2 films

Original Research Article
Pages 80-85
Kenkichiro Kobayashi, Takayori Koyama, Xinyu Zhang, Yoshiumi Kohono, Yasumasa Tomita, Yasuhisa Maeda, Shigenori Matsushima

Highlights

► Codoped ZnO films were grown by the alternate deposition of ZnO and Mg_3N_2 films. ► The band gap of the codoped ZnO films increases with the thickness of Mg-oxynitride films. ► p-type ZnO films were obtained by the deposition of sub-monolayer of Mg-oxynitride.

Electrical and magnetic properties of $CdRE_2W_2O_{10}$ tungstates (RE=Y,

Nd, Sm, Gd–Er)

Original Research Article
Pages 86-93
Z. Kukuła, E. Tomaszewicz, S. Mazur, T. Groń, S. Pawlus, H. Duda, T. Mydlarz

Graphical abstract

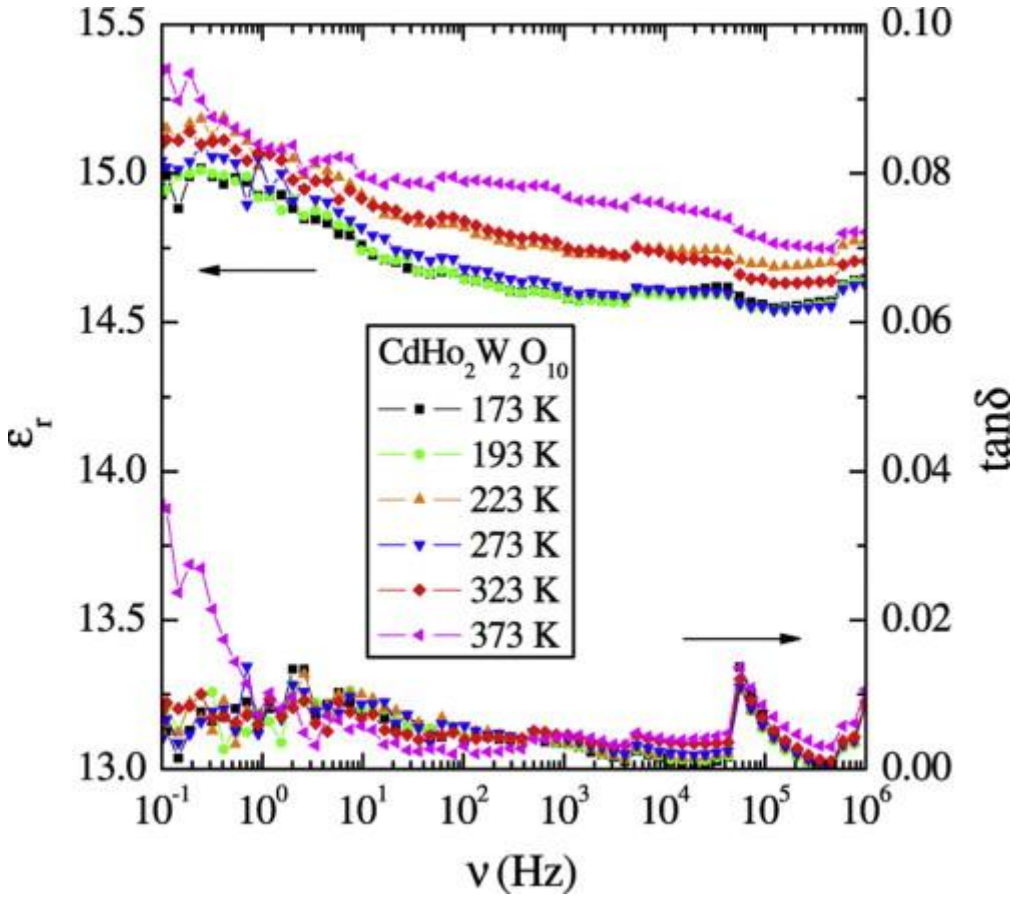

Highlights

► $CdRE_2W_2O_{10}$ tungstates are magnetically disordered insulators. ► The relative dielectric permittivity of $CdRE_2W_2O_{10}$ is typical for germanium. ► $CdNd_2W_2O_{10}$ and $CdGd_2W_2O_{10}$ show superparamagnetic-like behavior. ► The stronger orbital contribution, the weaker the superparamagnetic effect.

Pulsed laser deposition and characterization of highly tunable $(1-x)Ba(Zr_{0.2}Ti_{0.8})O_3–x(Ba_{0.7}Ca_{0.3})TiO_3$ thin films grown on $LaNiO_3$/Si substrate

Original Research Article
Pages 94-100

Chandan Bhardwaj, B.S.S. Daniel, Davinder Kaur

Highlights

► Pulsed Laser deposition of (1 0 0) oriented $(1-x)Ba(Zr_{0.2}Ti_{0.8})O_3–x(Ba_{0.7}Ca_{0.3})TiO_3$ on LNO/Si. ► Enhancement in electrical properties for BCZT50 (x=0.5) due to grain size effect and presence of MPB. ► Diffused phase transition behavior of $\varepsilon–T$ curve results in low TCC. ► BCZT50 thin film exhibits low leakage current with good fatigue endurance. ► BCZT50 could be a promising material for fabrication of tunable devices.

Monolithic porous graphitic carbons obtained through catalytic graphitization of carbon xerogels

Original Research Article
Pages 101-109
Wojciech Kiciński, Małgorzata Norek, Michał Bystrzejewski

Highlights

► Porous graphitic carbons were prepared using organic xerogels as substrates. ► Catalytic graphitization of the xerogels significantly enhances carbons' mesoporosity. ► Activation of the highly graphitic, mesoporous xerogels with KOH is investigated. ► The catalytic graphitization mechanism of the xerogels is discussed in details. ► A microstructure of the porous graphitic carbons is proposed.

Effect of reaction time on particle size and dielectric properties of manganese substituted $CoFe_2O_4$ nanoparticles

Original Research Article
Pages 110-114
E. Ranjith Kumar, R. Jayaprakash, T. ArunKumar, Sanjay Kumar

Highlights

► The higher combustion reaction time supports to achieve less particle size. ► The low value of dielectric loss is obtained by the influence of Manganese. ► Nature of the ferrites was affected with increasing annealing temperature.

Electrochemical properties of $LaMO_3$ (M=Co or Fe) as the negative electrode in a hydrogen battery

Original Research Article

Pages 115-120
D.-K. Lim, H.-N. Im, J. Kim, S.-J. Song

Highlights

► Performance of oxide anodes for Ni–H battery. ► Valence state of Fe and Co upon charging/discharging process. ► Hydrogen diffusion rate estimated by the potential-step method.

Effect of the glass composition on the chemical durability of zinc-phosphate-based glasses in aqueous solutions

Original Research Article
Pages 121-127
J. Massera, K. Bourhis, L. Petit, M. Couzi, L. Hupa, M. Hupa, J.J. Videau, T. Cardinal

Graphical abstract

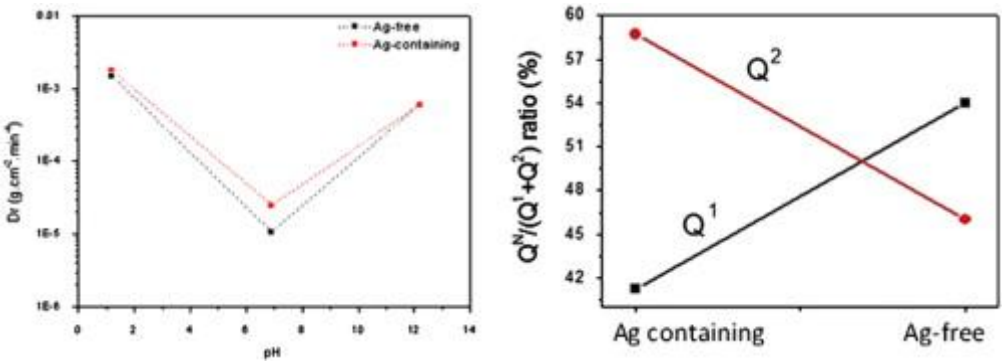

Highlights

► Leaching of the phosphate chains with the formation of a hydrated layer when immersed in neutral and acidic solutions. ► Consumption of the OH^- with the formation of $Zn_3(PO_4)_2{\cdot}(H_2O)_4$ and $Zn(H_2PO_2)_2{\cdot}H_2O$ layer when immersed in alkaline solution. ► Decrease of the dissolution rate with an increase of the Ga_2O_3 concentration at the expense of Ag_2O in zinc-phosphate glass.

Investigation of the H–Cu and Cu–Cu bonds in hydrogenated Cu

Original Research Article
Pages 128-134
I.G. Shuttleworth

Graphical abstract

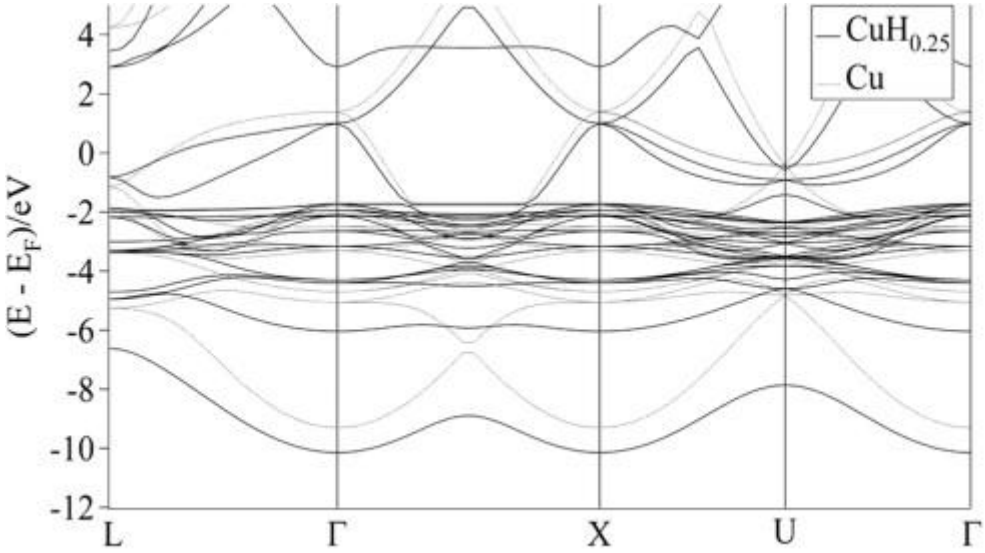

Band structure for the low H concentration $CuH_{0.25}$ and pure Cu systems

Highlights

► Preferential directional bonding in an environment that is expected to be highly non-directional. ► Increase (decrease) in the strength of the average H–Cu (Cu–Cu) interaction as hydrogenation increases. ► Formation of a occupied band gap for the low H concentration system $CuH_{0.25.}$

Influence of the fullerene derivatives and cage polyhedral oligomeric silsesqiuoxanes on 3-aminopropyltrimethoxysilane based hybrid nanocomposites chemical, morphological and electrical properties

Original Research Article
Pages 135-145
Jolanta Klocek, Krzysztof Kolanek, Karsten Henkel, Ehrenfried Zschech, Dieter Schmeisser

Highlights

► The combination of the surface-sensitive spectroscopic and microscopic methods. ► Fractal-shaped clusters formation. ► PCBM and POSS dopants decrease the dielectric constant of the produced composites.

Low temperature dc electrical conduction in reduced lithium niobate single crystals

Original Research Article
Pages 146-151
Ajay Dhar, Nidhi Singh, Rajiv K. Singh, Ramadhar Singh

Highlights

► The dc conductivity of $LiNbO_3$ crystals shows a peak with degree of reduction. ► This has been attributed to polaron hopping conduction mechanism. ► The dependence of dc conductivity of reduced $LiNbO_3$ crystals has also been studied. ► This temperature dependence has been explained by Mott's VRH conduction model.

Electrical resistivity and Curie temperature studies on $(Y_{1-x}Gd_x)(Fe_{0.7}Co_{0.3})_2$ intermetallics

Original Research Article
Pages 152-157
P. Guzdek, J. Pszczoła, J. Chmist, P. Stoch, P. Zachariasz, M. Onak

Highlights

► The contributions to total resistivity were separated for the $(Y_{1-x}Gd_x)(Fe_{0.7}Co_{0.3})_2$. ► The Debye temperatures were determined from measured resistivity. ► The Curie temperatures increases linearly with de Gennes factor. ► The magnetic ordering temperatures increases linearly with square of hyperfine fields.

Thermal strain and magnetization of the ferromagnetic shape memory alloy $Ni_{52}Mn_{25}Ga_{23}$ in a magnetic field

Original Research Article
Pages 158-165
T. Sakon, H. Nagashio, K. Sasaki, S. Susuga, D. Numakura, M. Abe, K. Endo, S. Yamashita, H. Nojiri, T. Kanomata

Highlights

► Thermal strain, permeability and magnetization measurements were performed on the Heusler alloy $Ni_{52}Mn_{25}Ga_{23}$. ► Steep decrease of the thermal strain due to the martensitic transition was obtained. ► Permeability abruptly changes around T_M and T_R. ► Temperature dependence of the magnetization also shows a clear discontinuity around T_M.

Structural and optical properties of ultrathin ZnO nanoneedles grown on GaN substrate by hybrid approach

Original Research Article
Pages 166-169
Ahsanulhaq Qurashi

Graphical abstract

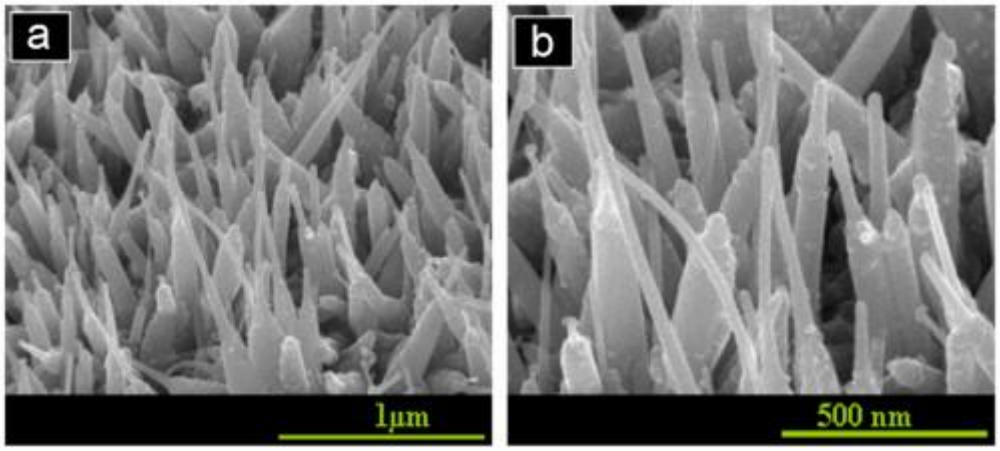

Highlights

► Low cost method is used for large-scale growth of ZnO nanoneedles on GaN. ► Structural and optical properties have been studied for ZnO nanoneedles grown on GaN. ► Nanoneedles have ultrathin nanotips which can be used for the fabrication of heterojunction. ► We used the low temperature hybrid method for the growth of ZnO nanoneedles on GaN.

Electron beam induced current imaging of dislocations in $Cd_{0.9}Zn_{0.1}Te$ crystal

Original Research Article
Pages 170-173
Ramesh M. Krishna, Peter G. Muzykov, Krishna C. Mandal

Highlights

► Electron beam induced current (EBIC) imaging has been carried out on detector grade CZT crystals. ► EBIC results have been correlated with defect delineating chemical etching results. ► Results suggest that the irregular shaped patterns are agglomerates of dislocations.